Supplemental Material:
First Measurement of Λ Electroproduction off Nuclei in the Current and Target Fragmentation Regions

T. Chetry,[29,13] L. El Fassi,[29,*] W. K. Brooks,[44,45,46,43] R. Dupré,[23] A. El Alaoui,[44] K. Hafidi,[1] P. Achenbach,[43] K.P. Adhikari,[29] Z. Akbar,[52] W.R. Armstrong,[1] M. Arratia,[48] H. Atac,[42] H. Avakian,[43] L. Baashen,[13] N.A. Baltzell,[43] L. Barion,[17] M. Bashkanov,[50] M. Battaglieri,[19] I. Bedlinskiy,[30] B. Benkel,[44] F. Benmokhtar,[10] A. Bianconi,[47,22] A.S. Biselli,[11,4] M. Bondi,[20] W.A. Booth,[50] F. Bossù,[6] S. Boiarinov,[43] K.-Th. Brinkmann,[36] W.J. Briscoe,[15] D. Bulumulla,[35] V.D. Burkert,[43] D.S. Carman,[43] J.C. Carvajal,[13] A. Celentano,[19] P. Chatagnon,[43,23] V. Chesnokov,[40,34] G. Ciullo,[17,12] P.L. Cole,[27,5,43] M. Contalbrigo,[17] G. Costantini,[47,22] A. D'Angelo,[20,39] N. Dashyan,[54] R. De Vita,[19] M. Defurne,[6] A. Deur,[43] S. Diehl,[36,8] C. Djalali,[34,41] H. Egiyan,[43] L. Elouadrhiri,[43] P. Eugenio,[14] S. Fegan,[50] A. Filippi,[21] G. Gavalian,[43,31] Y. Ghandilyan,[54] G.P. Gilfoyle,[38] D.I. Glazier,[49] A.A. Golubenko,[40] G. Gosta,[47] R.W. Gothe,[41] K.A. Griffioen,[53] M. Guidal,[23] L. Guo,[13] H. Hakobyan,[44] M. Hattawy,[35] T.B. Hayward,[8] D. Heddle,[7,43] A. Hobart,[23] M. Holtrop,[31] Y. Ilieva,[41] D.G. Ireland,[49] E.L. Isupov,[40] D. Jenkins,[51] H.S. Jo,[26] M. L. Kabir,[29] A. Khanal,[13] M. Khandaker,[33] A. Kim,[8] W. Kim,[26] F.J. Klein,[5] A. Kripko,[36] V. Kubarovsky,[43,37] V. Lagerquist,[35] L. Lanza,[20] M. Leali,[47,22] S. Lee,[1] P. Lenisa,[17,12] X. Li,[28] K. Livingston,[49] I.J.D. MacGregor,[49] D. Marchand,[23] V. Mascagna,[47,22] B. McKinnon,[49] C. McLauchlin,[41] Z.E. Meziani,[1,42] S. Migliorati,[47,22] T. Mineeva,[44] M. Mirazita,[18] V. Mokeev,[43] C. Munoz Camacho,[23] P. Nadel-Turonski,[43] K. Neupane,[41] S. Niccolai,[23] M. Nicol,[50] G. Niculescu,[25] M. Osipenko,[19] A.I. Ostrovidov,[14] P. Pandey,[35] M. Paolone,[32] L.L. Pappalardo,[17,12] R. Paremuzyan,[43,31] E. Pasyuk,[43] S.J. Paul,[48] W. Phelps,[7,15] N. Pilleux,[23] M. Pokhrel,[35] J. Poudel,[35] J.W. Price,[2] Y. Prok,[35,52] B.A. Raue,[13] T. Reed,[13] J. Richards,[8] M. Ripani,[19] J. Ritman,[16,24] G. Rosner,[49] F. Sabatié,[6] C. Salgado,[33] S. Schadmand,[16] A. Schmidt,[15,28] R.A. Schumacher,[4] Y.G. Sharabian,[43] E.V. Shirokov,[40] U. Shrestha,[8] P. Simmerling,[8] D. Sokhan,[6,49] N. Sparveris,[42] S. Stepanyan,[43] I.I. Strakovsky,[15] S. Strauch,[41,15] J.A. Tan,[26] N. Trotta,[8] R. Tyson,[49] M. Ungaro,[43,37] S. Vallarino,[17] L. Venturelli,[47,22] H. Voskanyan,[54] E. Voutier,[23] X. Wei,[43] L.B. Weinstein,[35] R. Williams,[50] R. Wishart,[49] M.H. Wood,[3,41] M. Yurov,[29] N. Zachariou,[50] Z.W. Zhao,[9,35] and M. Zurek[1]

(The CLAS Collaboration)

[1] *Argonne National Laboratory, Argonne, IL 60439*
[2] *California State University, Dominguez Hills, Carson, CA 90747*
[3] *Canisius College, Buffalo, NY 14208*
[4] *Carnegie Mellon University, Pittsburgh, PA 15213*
[5] *Catholic University of America, Washington, D.C. 20064*
[6] *IRFU, CEA, Université Paris-Saclay, F-91191 Gif-sur-Yvette, France*
[7] *Christopher Newport University, Newport News, VA 23606*
[8] *University of Connecticut, Storrs, CT 06269*
[9] *Duke University, Durham, NC 27708-0305*
[10] *Duquesne University, 600 Forbes Avenue, Pittsburgh, PA 15282*
[11] *Fairfield University, Fairfield CT 06824*
[12] *Universita' di Ferrara, 44121 Ferrara, Italy*
[13] *Florida International University, Miami, FL 33199*
[14] *Florida State University, Tallahassee, FL 32306*
[15] *The George Washington University, Washington, D.C. 20052*
[16] *GSI Helmholtzzentrum fur Schwerionenforschung GmbH, D-64291 Darmstadt, Germany*
[17] *INFN, Sezione di Ferrara, 44100 Ferrara, Italy*
[18] *INFN, Laboratori Nazionali di Frascati, 00044 Frascati, Italy*
[19] *INFN, Sezione di Genova, 16146 Genova, Italy*
[20] *INFN, Sezione di Roma Tor Vergata, 00133 Rome, Italy*
[21] *INFN, Sezione di Torino, 10125 Torino, Italy*
[22] *INFN, Sezione di Pavia, 27100 Pavia, Italy*
[23] *Universit'e Paris-Saclay, CNRS/IN2P3, IJCLab, 91405 Orsay, France*
[24] *Institut fur Kernphysik (Juelich), Juelich, 52428, Germany*
[25] *James Madison University, Harrisonburg, VA 22807*
[26] *Kyungpook National University, Daegu 41566, Republic of Korea*
[27] *Lamar University, 4400 MLK Blvd, PO Box 10046, Beaumont, TX 77710*
[28] *Massachusetts Institute of Technology, Cambridge, MA 02139-4307*
[29] *Mississippi State University, Mississippi State, MS 39762-5167*
[30] *National Research Centre Kurchatov Institute - ITEP, Moscow, 117259, Russia*

[31] *University of New Hampshire, Durham, NH 03824-3568*
[32] *New Mexico State University, PO Box 30001, Las Cruces, NM 88003, USA*
[33] *Norfolk State University, Norfolk, VA 23504*
[34] *Ohio University, Athens, OH 45701*
[35] *Old Dominion University, Norfolk, VA 23529*
[36] *II Physikalisches Institut der Universitaet Giessen, 35392 Giessen, Germany*
[37] *Rensselaer Polytechnic Institute, Troy, NY 12180-3590*
[38] *University of Richmond, Richmond, VA 23173*
[39] *Universita' di Roma Tor Vergata, 00133 Rome Italy*
[40] *Skobeltsyn Institute of Nuclear Physics, Lomonosov Moscow State University, 119234 Moscow, Russia*
[41] *University of South Carolina, Columbia, SC 29208*
[42] *Temple University, Philadelphia, PA 19122*
[43] *Thomas Jefferson National Accelerator Facility, Newport News, VA 23606*
[44] *Universidad Técnica Federico Santa María, Casilla, 110-V Valparaíso, Chile*
[45] *Center for Science and Technology of Valparaíso 699, Valparaíso, Chile*
[46] *SAPHIR Millennium Science Institute, Santiago, Chile*
[47] *Universit'a degli Studi di Brescia, 25123 Brescia, Italy*
[48] *University of California Riverside, 900 University Avenue, Riverside, CA 92521, USA*
[49] *University of Glasgow, Glasgow G12 8QQ, United Kingdom*
[50] *University of York, York YO10 5DD, United Kingdom*
[51] *Virginia Tech, Blacksburg, VA 24061-0435*
[52] *University of Virginia, Charlottesville, VA 22901*
[53] *College of William and Mary, Williamsburg, VA 23187-8795*
[54] *Yerevan Physics Institute, 375036 Yerevan, Armenia*

(Dated: March 10, 2023)

This document contains supplementary information about the Λ identification method in **SP.1**, the acceptance correction details related to the multidimensional (6D) map variables and binning, weight definition and cut, and its application procedure in **SP.2**, a summary of the contributions of systematic effects to the total point-to-point uncertainty budget in **SP.3**, and the reported results in the last two figures, Figs. 3 and 4, of the "**First Measurement of Λ Electroproduction off Nuclei in the Current and Target Fragmentation Regions**" PRL manuscript as well as two supporting figures, Figs. S1 and S2, in **SP.4**. In Table S6, the z-binned multiplicity ratios are given for all nuclei, while Table S7 (Table S8) contains the transverse momentum broadening as a function of z (A) for all nuclei.

SP.1 Lambda Identification In the sample of reconstructed SIDIS events originating from either the liquid or solid target, one scattered e^- and at least one π^- and p, the decay products of the Λ, were required. To reconstruct the z-binned (π^-, p) invariant mass spectrum for each target, the 4-vector energy-momentum ($P^\mu = (E, p_x, p_y, p_z)$) of all identified negatively charged pions and protons were combined event-by-event as

$$P_\Lambda = P_p + P_{\pi^-}, \tag{S1}$$

where P_Λ, P_p, and P_{π^-} are the 4-vector energy-momentum of the Λ candidates, protons, and π^-s, respectively. Figure 2 left shows the acceptance-weighted invariant mass from solid (top) and liquid (bottom) targets in which the Λ peak sits on a huge combinatorial background (red dotted curves) that is subtracted using `RooFit` to extract the pure Λ yields and thus obtain the presented multiplicity ratios in Fig. 3.

SP.2 Acceptance Correction The adopted acceptance correction for this analysis is based on a bin-by-bin correction method. Its main advantage is that it should be, in principle, independent of the model used in the Monte-Carlo (MC) event generator if the chosen bins are infinitely small. This is very important for this channel since it is not expected that the employed model in Pythia would be realistic enough to perfectly reproduce the data. Based on a comparison between MC and experimental data, the chosen AC six dimensional (6D) map variables and binning are summarized in Tables S1- S2.

Variables	Range	Number of bins	Bin width
W [GeV]	2.00 - 2.80	2	0.4
ν	2.25 - 4.25	3	$0.\overline{6}$
ϕ_{π^-} [deg]	0.0 - 360.0	2	180
$\phi_{e\Lambda}$ [deg]	0.0 - 360.0	3	120
P_Λ [GeV]	0.10 - 4.25	3	$1.38\overline{3}$
z	0.28 - 1.00	6	see Table S2
Total		648	

Table S1. Binning for the AC map, where ν, W, and z were already defined, ϕ_{π^-} is the π^- azimuthal decay angle in the Λ rest frame, $\phi_{e\Lambda}$ is the angle between the leptonic and hadronic planes, and p_Λ is the Λ momentum. Table S2 shows the z bins used as reported in Table S6.

$z-$bin #	1	2	3	4	5	6
z_{min}	0.28	0.38	0.44	0.51	0.60	0.75
z_{max}	0.38	0.44	0.51	0.60	0.75	1.00

Table S2. The z bins used in this analysis.

The acceptance correction factors are defined for each 6D bin k= (W, ν, p_Λ, ϕ_{π^-}, $\phi_{e\Lambda}$, z) as

$$AC_k = \frac{N_{acc}(W, \nu, p_\Lambda, \phi_{\pi^-}, \phi_{e\Lambda}, z)}{N_{gen}(W, \nu, p_\Lambda, \phi_{\pi^-}, \phi_{e\Lambda}, z)}, \tag{S2}$$

where $N_{gen}(W, \nu, p_\Lambda, \phi_{\pi^-}, \phi_{e\Lambda}, z)$ and $N_{acc}(W, \nu, p_\Lambda, \phi_{\pi^-}, \phi_{e\Lambda}, z)$ are, respectively, the number of generated and accepted events in each bin k. Once these AC coefficients were computed, the data were corrected event-by-event by a weight $\omega_k = 1/AC_k$, which depends on the bin k to which it belongs. It should be noted that if some 6D AC bins have very small correction factors due to their poor statistics, an artificially large weight would be attributed to those bins that would lead to spikes in the weighted distributions. To avoid this problem, the following weight cut was adopted to minimize this effect on the weighted distributions:

$$60 < \omega_k \leq 2400. \tag{S3}$$

Furthermore, the effect of this weight cut was estimated and applied as a global correction factor, f_ω, to the extracted results. This estimation was done by weighting the MC accepted N_{acc} events and comparing their sum, $\sum \omega N_{acc}$, to the generated ones as

$$f_\omega = \frac{\sum \omega N_{acc}}{N_{gen}.} \tag{S4}$$

This N_{acc} weighted sum is typically equal to the generated events without the weight cut, however, it is slightly less once applied, leading to various f_ω corrections for each z-binned multiplicity ratio result as the p_T-broadening means are insensitive to this correction.

SP.3 Systematic Uncertainties Budget This section contains the contribution of various systematic effects to the reported total point-to-point systematic uncertainty budget for the Λ multiplicity ratios of all nuclei in Table S3 and the corresponding z (A) dependence of p_T-broadening in Table S4 (S5).

SP.4 Tabulated Multiplicity Ratio and p_T-broadening Results This section contains the reported results in the last two figures, Figs. 3 and 4, of the "**First Measurement of Λ Electroproduction off Nuclei in the Current and Target Fragmentation Regions**" PRL manuscript, detailed in Table S6 for all nuclei z-binned multiplicity ratios, and Table S7 (Table S8) for all nuclei z-binned (A-dependent) transverse momentum broadening. In addition, the correlation between z and the Feynman variable x_F is illustrated in Fig. S1 to support the discussion related to the separation between forward and backward fragmentation regions. Furthermore, the z-binned distributions, as well as AC-weighted averages, of the Bjorken scaling variable x_B are shown in Fig. S2 and Table S9 to illustrate our kinematical coverage for any theoretical calculations aiming to describe our data.

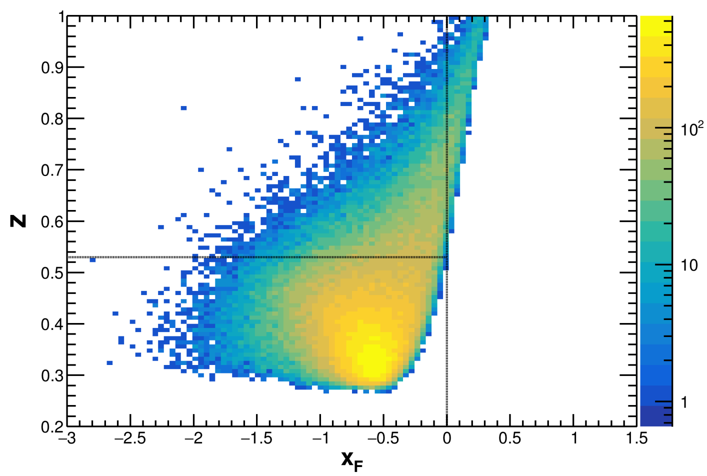

Figure S1. z vs. x_F, where the horizontal dashed line around values of z greater than ∼0.55 depicts the discussed separation between forward and backward fragmentation regions suggested by the sign change of x_F (vertical dashed line).

* le334@msstate.edu

Table S3. Multiplicity ratio systematic effects and their contributions for the z-bins shown in Table S2.

Systematic Effect	z-bin Point-to-point Systematic Uncertainty (%)																	
	Carbon						Iron						Lead					
	z−1	z−2	z−3	z−4	z−5	z−6	z−1	z−2	z−3	z−4	z−5	z−6	z−1	z−2	z−3	z−4	z−5	z−6
Particle identification cuts	0.69	4.24	7.24	1.53	3.16	0.00	0.00	0.95	4.34	0.87	3.17	4.45	8.05	3.21	7.80	0.00	8.59	6.91
Vertex corrections	0.28	0.00	0.04	0.22	0.22	0.54	1.04	1.28	0.56	0.08	0.00	0.13	1.38	1.85	0.13	0.18	0.00	1.01
AC 6D map variables & binning	3.28	0.00	6.69	9.97	9.17	2.33	6.83	4.80	0.00	6.42	5.90	4.93	6.84	0.00	9.05	7.90	6.06	7.23
AC weight cuts	0.00	0.00	10.70	0.70	0.00	0.00	0.00	0.00	9.17	1.86	0.00	0.00	5.17	0.00	8.64	12.16	0.00	0.00
CB uncorrelated-tracks combinations	1.80	0.16	0.37	0.27	0.53	0.00	1.14	0.14	0.20	0.00	0.36	0.23	1.79	2.04	0.96	0.13	0.00	0.28
Breit-Weigner shapes	7.55	10.80	25.75	5.13	8.69	5.77	20.54	16.37	13.40	1.26	0.46	5.27	5.77	12.02	15.71	4.92	10.85	9.52
Λ mass-range	2.10	1.11	0.00	0.86	1.87	2.89	2.52	1.52	0.43	0.00	1.35	2.39	2.24	1.24	0.00	0.65	1.69	2.72
LD2 endcaps	0.06	0.00	0.06	0.09	0.11	0.13	0.03	0.00	0.06	0.08	0.10	0.12	0.07	0.00	0.05	0.07	0.09	0.13
Radiative correction	0.00	2.08	1.26	3.18	1.53	0.94	1.30	1.14	0.29	0.00	0.95	0.21	0.13	0.00	0.81	1.12	0.58	1.90
Total	8.71	11.84	29.61	11.81	13.25	6.93	21.86	17.19	16.82	6.86	6.92	8.81	13.41	12.67	21.58	15.36	15.21	14.20

Table S4. Transverse momentum broadening systematic effects and their contributions for the z-bins shown in Table S2.

Systematic Effect	z-bin Point-to-point Systematic Uncertainty (%)																	
	Carbon						Iron						Lead					
	$z-1$	$z-2$	$z-3$	$z-4$	$z-5$	$z-6$	$z-1$	$z-2$	$z-3$	$z-4$	$z-5$	$z-6$	$z-1$	$z-2$	$z-3$	$z-4$	$z-5$	$z-6$
Particle identification cuts	7.14	0.00	3.77	1.77	0.47	6.03	1.05	8.19	4.97	0.00	0.82	0.87	5.07	2.84	6.24	0.00	3.52	3.24
Vertex Corrections	6.63	8.99	4.62	1.02	0.00	3.99	2.57	2.54	0.00	0.33	0.33	0.67	3.40	1.87	0.81	0.00	0.74	2.79
AC 6D map variables & binning	4.77	6.95	6.02	0.00	8.91	5.49	6.36	9.72	3.05	14.85	0.00	2.20	9.84	7.83	10.52	3.83	7.73	0.00
AC weight cuts	1.83	0.47	18.23	6.74	0.00	0.09	0.00	0.31	13.77	1.52	0.00	0.12	20.17	0.59	19.88	23.63	0.08	0.00
CB sideband subtraction	31.84	0.0	2.1	8.81	0.88	3.79	4.34	2.36	0.0	1.67	7.58	20.32	77.31	8.16	0.0	2.49	6.33	13.28
Radiative correction	3.87	0.24	0.00	0.03	0.00	0.19	0.18	0.28	0.32	0.54	0.00	0.12	5.06	0.49	0.27	0.01	0.00	0.00
Total	33.88	11.38	20.21	11.28	8.96	9.84	8.19	13.18	14.96	15.04	7.63	20.46	80.89	11.84	23.35	24.07	10.62	13.95

Table S5. A-dependent transverse momentum broadening systematic effects and their contributions.

Systematic effect	Point-to-point Systematic Uncertainty (%)		
	Carbon	Iron	Lead
Particle identification cuts	4.69	1.35	0.00
Vertex Corrections	2.70	0.00	0.38
AC 6D map variables & binning	0.57	0.00	2.21
AC weight cuts	3.40	0.00	7.07
CB sideband subtraction	5.52	0.0	2.87
Radiative correction	0.04	0.17	0.00
Total	8.46	1.36	7.96

Table S6. Measured Λ z-binned multiplicity ratios for all nuclei along with their total statistical and systematic (point-to-point and normalization uncertainties depicted in Fig. 3 added in quadrature) uncertainties.

z-bin	R^A_Λ $\pm$ Statistical $\pm$ Systematical Uncertainties		
	Carbon	Iron	Lead
0.28 - 0.38	3.4256 $\pm$ 0.5319 $\pm$ 0.3004	5.7536 $\pm$ 0.5681 $\pm$ 1.2661	7.2363 $\pm$ 0.9997 $\pm$ 0.9893
0.38 - 0.44	1.3447 $\pm$ 0.1603 $\pm$ 0.1628	1.9382 $\pm$ 0.1769 $\pm$ 0.3629	2.6378 $\pm$ 0.3405 $\pm$ 0.3863
0.44 - 0.51	1.1084 $\pm$ 0.1205 $\pm$ 0.3299	2.0100 $\pm$ 0.1735 $\pm$ 0.3674	2.1293 $\pm$ 0.2316 $\pm$ 0.4987
0.51 - 0.60	1.1498 $\pm$ 0.0883 $\pm$ 0.1400	1.2126 $\pm$ 0.0823 $\pm$ 0.1663	1.1857 $\pm$ 0.1057 $\pm$ 0.2659
0.60 - 0.75	1.1174 $\pm$ 0.0756 $\pm$ 0.1519	0.9660 $\pm$ 0.0617 $\pm$ 0.1588	0.8910 $\pm$ 0.0759 $\pm$ 0.2364
0.75 - 1.00	0.9506 $\pm$ 0.1011 $\pm$ 0.0741	0.6450 $\pm$ 0.0529 $\pm$ 0.1549	0.5622 $\pm$ 0.0621 $\pm$ 0.2096

Table S7. Measured Λ z-binned p_T-broadening results for all nuclei with their total statistical and systematic (point-to-point and normalization uncertainties depicted in Fig. 4 left added in quadrature) uncertainties.

z-bin	Δp_T^2 (GeV^2) $\pm$ Statistical $\pm$ Systematical Uncertainties		
	Carbon	Iron	Lead
0.28 - 0.38	0.0003 $\pm$ 0.0143 $\pm$ 0.0015	0.0112 $\pm$ 0.0127 $\pm$ 0.0015	-0.0072 $\pm$ 0.0151 $\pm$ 0.0060
0.38 - 0.44	0.0259 $\pm$ 0.0160 $\pm$ 0.0033	0.0422 $\pm$ 0.0140 $\pm$ 0.0057	0.0592 $\pm$ 0.0171 $\pm$ 0.0071
0.44 - 0.51	0.0648 $\pm$ 0.0174 $\pm$ 0.0132	0.0894 $\pm$ 0.0147 $\pm$ 0.0134	0.0613 $\pm$ 0.0174 $\pm$ 0.0144
0.51 - 0.60	0.1317 $\pm$ 0.0165 $\pm$ 0.0149	0.2120 $\pm$ 0.0168 $\pm$ 0.0319	0.2007 $\pm$ 0.0211 $\pm$ 0.0483
0.60 - 0.75	0.1879 $\pm$ 0.0225 $\pm$ 0.0169	0.2591 $\pm$ 0.0218 $\pm$ 0.0198	0.3140 $\pm$ 0.0295 $\pm$ 0.0334
0.75 - 1.00	0.1145 $\pm$ 0.0157 $\pm$ 0.0114	0.1381 $\pm$ 0.0149 $\pm$ 0.0283	0.1788 $\pm$ 0.0209 $\pm$ 0.0250

Table S8. Measured Λ A-dependent p_T-broadening results for all nuclei along with their total statistical and systematic (point-to-point and normalization uncertainties depicted in Fig. 4 right added in quadrature) uncertainties.

A	Δp_T^2 (GeV^2) $\pm$ Statistical $\pm$ Systematical Uncertainties
Carbon	0.0952 $\pm$ 0.0272 $\pm$ 0.0082
Iron	0.1404 $\pm$ 0.0376 $\pm$ 0.0024
Lead	0.1823 $\pm$ 0.0451 $\pm$ 0.0146

Table S9. z-binned x_B AC-weighted averages for all nuclei.

z-bin	x_B AC-weighted Average			
	LD2	Carbon	Iron	Lead
0.28 - 0.38	0.2176	0.2395	0.2401	0.2391
0.38 - 0.44	0.2529	0.2574	0.2623	0.2551
0.44 - 0.51	0.2585	0.2665	0.2701	0.2724
0.51 - 0.60	0.2661	0.2699	0.2697	0.2703
0.60 - 0.75	0.2756	0.2648	0.2667	0.2646
0.75 - 1.00	0.2921	0.2858	0.2821	0.2817

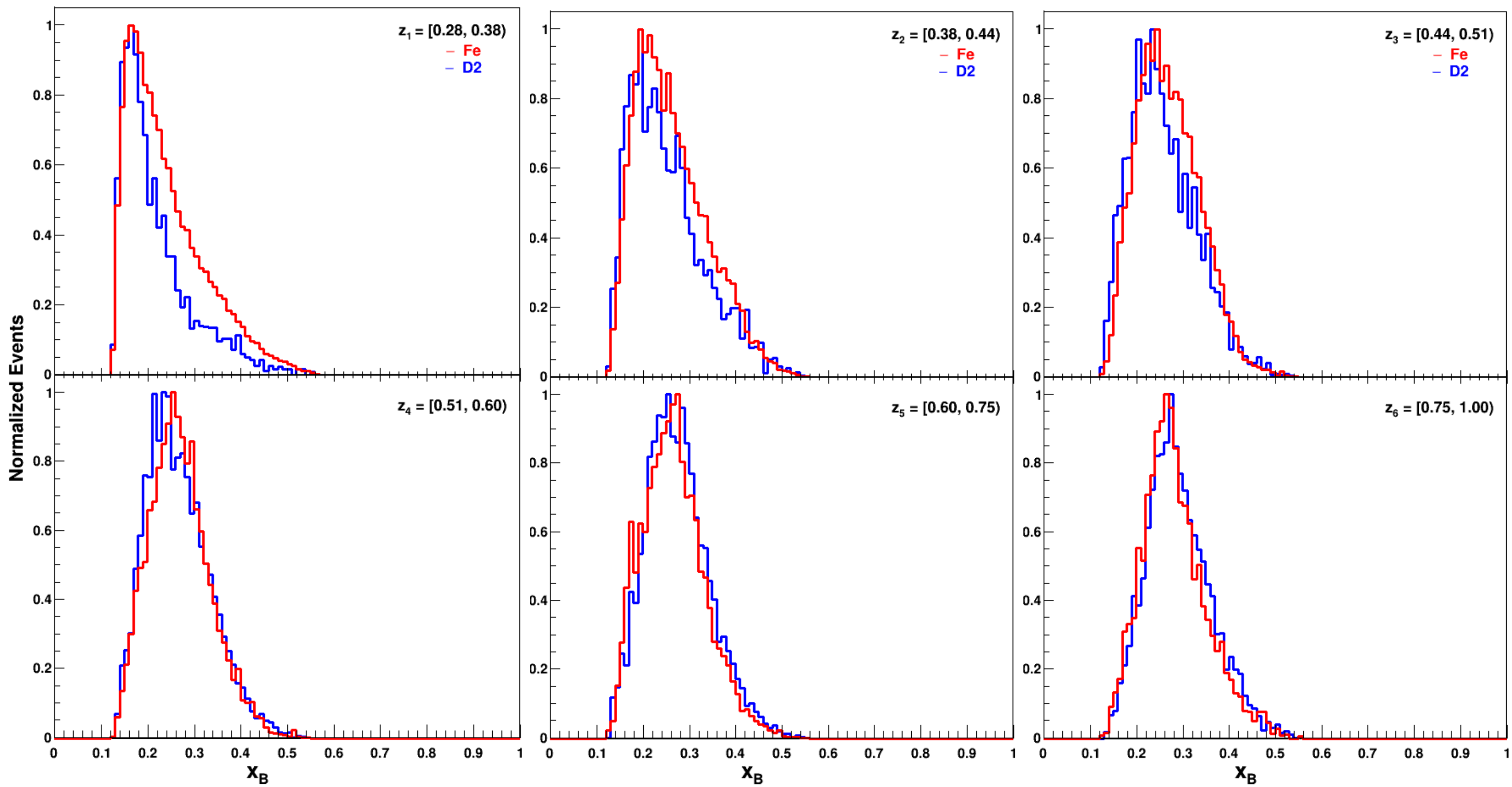

Figure S2. Comparison of the z-binned Fe (red) and LD2 (blue) normalized acceptance-weighted x_B distributions for the depicted z bins that are defined in Table S2.